Finding the Bed Shear Stress on a Rough Bed Using the Log Law

Francis C. K. Ting, M.ASCE[1]; and Gunnar S. Kern[2]

Abstract: The procedure commonly used to determine the friction velocity from a measured velocity profile in turbulent flow over a hydraulically rough bed is to fit the log law to the velocity profile and adjust the displacement height to obtain a best-fit line to as many data points as possible in the inner layer. In practice, the process can be subjective and produce large uncertainty in the bed shear stress estimates and/or inconsistent results for the equivalent roughness height. In oscillatory flows, a temporal variation in the equivalent grain roughness is unrealistic because the roughness height should remain constant if the boundary Reynolds number is sufficiently large. An alternative method is presented in this study, in which the equivalent grain roughness is held constant, and the displacement height is varied until the value of the von Kármán constant obtained from the best-fit line is equal to the universally accepted value of about 0.4. The iterative process converges rapidly and is easier to apply than the traditional method, which requires the displacement height to be found by trial and error. The method was tested in steady, shallow uniform flows over a fixed bed of fine gravel. The channel slope was varied, and the velocity profile was measured using the particle image velocimetry (PIV) technique. Good agreement was found between the bed shear stress estimates obtained using the new method and the values calculated from the measured flow depth and channel slope when the k_s/d_{90} ratio was taken from the literature for small values of the h/d_{90} ratio, where h is the flow depth, k_s is the equivalent roughness height, and d_{90} is the grain diameter with 90% of finer particles, therefore verifying that the new method produced results consistent with published data. The method was then applied to velocity measurements under a solitary wave to obtain the temporal variation of bed shear stress on a gravel bed near the point of incipient wave breaking. **DOI: 10.1061/(ASCE)WW.1943-5460.0000707**.

Introduction

The velocity distribution in the inner layer of a steady, turbulent, two-dimensional flow over a hydraulically rough bed may be represented by a logarithmic profile (Middleton and Southard 1984)

$$\frac{u}{u^*} = A \ln\left(\frac{y - y_0}{k_s}\right) + B \tag{1}$$

where u = time-averaged velocity at a distance y from a reference level; y_0 = elevation of the theoretical bed (displacement height); u^* = friction velocity; $A = 1/\kappa$ ($\kappa \approx 0.4$ is the von Kármán constant); k_s = equivalent grain roughness; and B is a constant whose value depends on the nature of the bed surface. The logarithmic profile is also found in oscillating water tunnels (Sleath 1987; Jensen et al. 1989; van der A et al. 2011; Yuan and Madsen 2014; O'Donoghue et al. 2021) and under surface waves (Cox et al. 1996; Dixen et al. 2008; Xie et al. 2021), where u denotes the phase- or ensemble-averaged velocity. However, obtaining reliable estimates of bed shear stress from measured velocity profiles using the log law is nontrivial, especially in unsteady flows in which the bed shear stress varies with time.

To determine the bed shear stress τ_b ($=\rho u^{*2}$, ρ is the fluid density) from a measured velocity profile, it is customary to assume a value of 8.5 for B which was originally obtained by Nikuradse (1933) for uniform, close-packed sand grains. A plot of $\ln(y - y_0)$ versus u is created, and the value of y_0 is adjusted to produce the best straight-line fit to as many data points as possible in the region where the logarithmic profile is supposed to exist. The latter is commonly taken as $0.2k_s \lesssim y - y_0 \lesssim (0.2 - 0.3)h$, where h is the flow depth (Sumer and Fuhrman 2020). The friction velocity u^* is then found from the slope ($=\kappa/u^*$) of the best-fit line and the equivalent grain roughness k_s from the y-intercept ($=\ln k_s - 8.5\kappa$). In practice, finding the value of y_0 can be subjective, with significant effects on the results for u^* and k_s (Zarrati and Jin 2004). Kamphuis (1974) assumed y_0 to be at 0.7 d_{90} above the plane to which the grains were adhered, and for a wide range of h/d_{90} ratios in uniform flows, he found that the value of k_s/d_{90} ranges from 0.78 to 2.6, where d_{90} is the grain diameter with 90% of finer particles. Sumer and Fuhrman (2020) compiled a list of k_s values collected from different studies. The list includes a large channel paved with boulders in which the value of k_s was found to be as large as $4.5d_{90}$. In oscillatory flows, a temporal variation in the value of k_s over the wave cycle is considered unrealistic if the boundary layer is fully developed and the bed is hydraulically rough (Cox et al. 1996). To resolve this problem, van der A et al. (2011) averaged the values of y_0 and k_s obtained from the velocity profile of the amplitude of the first harmonic for experiments with the same bed type. With the average values of y_0 and k_s established, they then obtained the intrawave friction velocity u^* by fitting Eq. (1) to the measured instantaneous velocity profiles.

In this paper, we examine a different approach for finding τ_b from the measured velocity profiles. Instead of treating k_s as an unknown that is obtained with u^* and y_0 when determining the best straight-line fit to Eq. (1), k_s is held constant and the displacement

[1]Professor, Dept. of Civil and Environmental Engineering, South Dakota State Univ., Brookings, SD 57007 (corresponding author). ORCID: https://orcid.org/0000-0001-8524-7691. Email: francis.ting@sdstate.edu

[2]Graduate Student, Dept. of Civil and Environmental Engineering, South Dakota State Univ., Brookings, SD 57007.

Note. This manuscript was submitted on May 30, 2021; approved on February 1, 2022; published online on April 29, 2022. Discussion period open until September 29, 2022; separate discussions must be submitted for individual papers. This paper is part of the ***Journal of Waterway, Port, Coastal, and Ocean Engineering***, © ASCE, ISSN 0733-950X.

height y_0 is varied until the value of κ obtained from the y-intercept of the best-fit line is equal to 0.4. The results are first presented for steady, shallow (supercritical) uniform flows with h/d_{90} ratio $\lesssim 5$. We find that the value of u^* obtained using the new method is relatively insensitive to known variations in the κ and y_0 values selected. By matching the bed shear stress estimates obtained using this method with the values calculated from the measured flow depth and channel slope, we find that the values of the k_s/d_{90} ratio are about the same as those given in Kamphuis (1974), therefore verifying that the new method produces results consistent with published data. We then apply the new method to the measured velocity profiles under a solitary wave to obtain the temporal variation of bed shear stress on a gravel bed near the point of incipient wave breaking.

Law of the Wall

The velocity gradient in the inner layer down to where the flow is not influenced by the individual grain particles can be written in the form (Middleton and Southard 1984)

$$\frac{du}{dy} = \frac{Au^*}{y - y_0} \tag{2}$$

This equation assumes that the velocity gradient in the inner layer depends on τ_b, ρ, and y but not on the particle diameter D, flow depth h, and fluid viscosity μ. Upon integration, Eq. (2) yields Eq. (1) with the constant of integration B. The latter is a function of the boundary Reynolds number (based on D for uniform grains or k_s for nonuniform grains) because the fluid velocity itself must depend on the grain size. The displacement height y_0 depends in a complicated way on the nature of the bed surface and is usually found by trial and error. Rearranging Eq. (1) with $A = 1/\kappa$, we get

$$\ln(y - y_0) = \frac{\kappa}{u^*} u + (\ln k_s - \kappa B) \tag{3}$$

which yields a straight line with slope of κ/u^* and y-intercept of $\ln k_s - \kappa B$ on a plot of $\ln(y - y_0)$ versus u. The desired value of y_0 is that which produces the best straight-line fit to Eq. (3) with as many data points as possible in the inner layer. The latter is supposed to lie in a region up to 20%–30% of the flow depth above the bed. Eq. (2) shows that for a given set of measured velocity points, the value of u^* obtained from the best-fit line must increase as y_0 decreases. Then, Eq. (3) shows that the y-intercept, $\ln k_s - \kappa B$, must increase because y_0 decreases and u^* increases. This will, in turn, cause k_s to increase if κ and B are held constant. Hence, varying y_0 by trial and error while searching for a best-fit line can easily produce large values of k_s that are physically unrealistic.

The concept of equivalent bed roughness may be examined by rewriting Eq. (1) in the following form (see also Middleton and Southard 1984):

$$\frac{u}{u^*} = \frac{1}{\kappa} \ln\left(\frac{y - y_0}{D}\right) + 8.5 + \frac{1}{\kappa} \ln\left(\frac{1}{\alpha}\right) \tag{4}$$

where the last term is a correction to the value of $B = 8.5$ found for uniform grains, and α is a constant whose value depends on the nature of the bed surface such as the grain size distribution. Here, D is a representative grain size such as the d_{50}. The factor α can be combined with D to produce an equivalent grain roughness $k_s = \alpha D$ as shown in Eq. (1). Like the value of 8.5 for uniform grains, α should remain constant for a given bed surface if the boundary Reynolds number is sufficiently large. Hence, setting k_s equal to a constant with $B = 8.5$ in Eq. (3), y_0 may be varied systematically until the value of κ obtained from the y-intercept of the best-fit line is equal to 0.4. The value of u^* can then be found from the slope of the best-fit line. This approach is different from the procedure used by van der A et al. (2011), who kept the values of both k_s and y_0 constant while fitting the logarithmic profile to the intrawave velocity profiles. In Eq. (2), $y - y_0$ represents the length scale of the large eddies involved in turbulent momentum transfer that determines the velocity gradient of the mean flow. Unlike k_s, there is no reason why the length scale of the large eddies should remain constant over a wave cycle. It will also be seen that the value of τ_b obtained using the new method depends primarily on the value of k_s selected and is relatively insensitive to the values of y_0 and κ.

The procedure for finding u^* is as follows. Starting with y_0 at a fraction of d_{90} below the top of the rough bed, the value of y_0 is increased in small increments. From Eq. (2), the value of κ/u^* given by the slope of the best-fit line will increase as $y - y_0$ decreases. Then, Eq. (3) shows that the y-intercept ($=\ln k_s - \kappa B$) of the best-fit line will decrease. The value of κ calculated from the y-intercept will increase because k_s and B are held constant. The desired value of y_0 is reached when the value of κ is equal to 0.4. The friction velocity u^* is then found from the slope of the best-fit line. The method is applied to the measured velocity profiles in steady, uniform flows and in a solitary wave to find the bed shear stress over a fixed gravel bed.

The method described here assumes that the value of k_s is known. For a uniform flow in an open channel, the bed shear stress may also be found from the measured flow depth and channel slope. By comparing those results with the bed shear stress estimates obtained using the log law, we can then determine the value of k_s for a given bed type. Published values of k_s/d_{90} in open-channel flows are given in Kamphuis (1974) for a wide range of h/d_{90} ratio. He found that the value of k_s/d_{90} may be taken as 2.5 when the h/d_{90} ratio is greater than 15 but decreases rapidly with the h/d_{90} ratio when $h/d_{90} < 10$. His measured data in this range include two data points: the value of k_s/d_{90} is 1.5 at $h/d_{90} = 9.3$ and 0.78 at $h/d_{90} = 3.0$ (see Table 1 in his paper). His measurements indicate that flow depth is an important parameter at small values of the h/d_{90} ratio. In this study, new tests were carried out in a tilting flume to determine the values of k_s/d_{90} over a range of h/d_{90} ratios between 3.4 and 5.3. The new measurements may be considered complementary to the experimental data by Kamphuis (1974) at the low end of the h/d_{90} ratio and provide a check on the new method.

For the solitary wave, the log law was first fitted to the measured velocity profile at the wave crest phase to determine the value of k_s as in van der A et al. (2011) and O'Donoghue et al. (2021). This value was then applied with the new method to the instantaneous

Table 1. Grain size distribution of gravel

r% of finer particles	d_r (mm)
10	3.5
20	4.1
30	4.6
40	5.1
50	5.6
60	6.0
65	6.1
70	6.3
80	6.8
84	7.0
90	7.4

Note: The values of d_r are interpolated from Fig. 1.

velocity profiles to determine the temporal variation of bed shear stress.

Procedure for Steady Flow Experiment

The steady flow experiment was conducted in an A-8 hydraulic flume manufactured by Engineering Laboratory Design (ELD). The working channel is 0.15-m wide with 0.3-m depth and 2.44-m length fabricated of a 13-mm-thick clear acrylic. The channel slope is continuously adjustable to +12% and measured using a digital inclinometer with a precision of ±0.1%. Flow discharge is regulated by a gate valve and measured using an orifice meter connected to a low-range differential pressure transducer manufactured by Validyne. Flow depth is controlled by a manually operated tail gate and measured using a point gage with a precision of ±0.1 mm. The entrance to the flume is covered by a perforated metal screen to prevent the formation of large-scale disturbances.

The rough bed was constructed by gluing a single layer of fine gravel with a d_{50} of 5.6 mm on 5-mm-thick acrylic sheets using epoxy resin. Loose gravels were removed with a brush after drying. The grain size distribution was determined by sieve analysis. The average results from five trials are plotted in Fig. 1 and fitted with a smoothing spline. The interpolated d_r values are presented in Table 1. The acrylic sheets were fastened to the flume floor using metal screws and in-floor threaded inserts. The gap between the acrylic sheet and the side wall was about 1 mm.

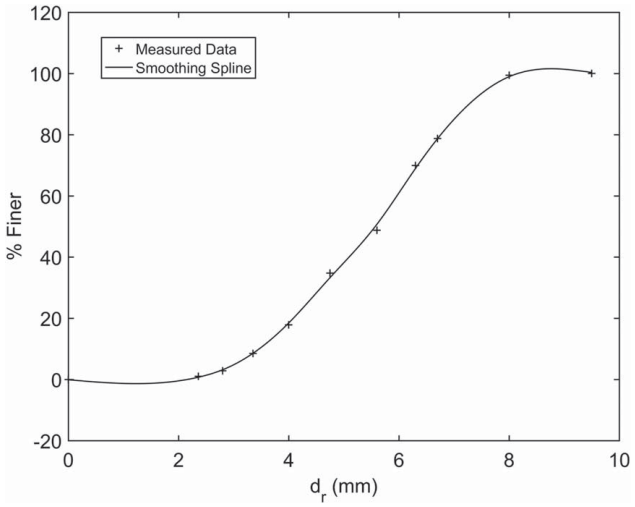

Fig. 1. Grain size distribution of gravel.

The flow conditions on a granular bed made of a single layer of particles adhered to a plane surface are different from those on a natural stream or a movable bed with multiple layers of loose particles. The latter would exhibit a much wider range of k_s values due to the heterogeneity of the sediment, micro-topography, bedforms, and bed load transport (López and Barragán 2008). Therefore, the results from this study may not be compared directly with field data collected in a natural gravel-bed stream. Our experiment involved supercritical flows over a hydraulically rough but otherwise plane bed on a steep slope. The flow conditions may be like the uprush or downwash on an armored bed or a gravel beach when ripples are washed away by high flow velocities.

The test conditions are shown in Table 2. There were six different flow conditions created by varying the channel slope from 2% to 10%. All the tests were conducted under a uniform flow condition at a constant discharge of 4.5 L/s. The tail gate was lowered, and the backwater effect was avoided by creating supercritical flow ($F > 1$). The uniform depth h was taken as the flow depth measured from the acrylic sheet. The effective depth of water above the gravel bed h_e, which represents the weight of water transmitted as bed shear stress, was calculated as $h-(1-n)d_{50}$, where n is the porosity of the gravel layer. The h/d_{90} ratios of the flume tests ranged from 3.4 to 5.3, which were at the low end of the values investigated by Kamphuis (1974). In all the tests, the bulk Reynolds number Re was around 10^5 and the boundary Reynolds number Re^* was much larger than 60. Therefore, the flows were fully turbulent, and the bed was hydraulically rough.

For a steady, uniform flow, the bed shear stress may also be calculated from the measured flow depth and channel slope. The results are presented in Table 2. The sidewall correction method in Cheng (2011) was used to estimate the bed-related friction factor f_b and hydraulic radius R_b. The bed shear stress τ_b was then calculated as $\rho g R_b S$ (see Appendix), where ρ is the fluid density, g is the acceleration of gravity, and S is the channel slope. Loosely packed gravel may have a porosity of 0.4 (Frings et al. 2011), but the void fraction of a single layer of gravel is likely to be higher. Note that the calculated bed shear stress is insensitive to the porosity of the gravel bed assumed. For example, with $n = 0.5$, the value of τ_b on a 10% slope is 20.6 N/m^2 (Test 10, Table 2). With $n = 0.4$ and 0.6, the corresponding values are 20.1 and 21.2 N/m^2. A value of 0.5 was assumed for n in this study.

Velocity measurements over the gravel bed were obtained using a PIV system manufactured by TSI Incorporated. The flow was seeded with latex particles (mean diameter = 55 μm, specific gravity = 1.016). Instead of the 200 mJ Dual Nd:YAG laser normally used with the PIV system, the flow field was illuminated using a model IL-105X high-power-LED illuminator manufactured by the HARDsoft Microprocessor system. The use of LED light

Table 2. Summary of flow parameters in the steady flow experiment

Test	No. runs	S	T (°C)	h (mm)	h_e (mm)	V (m/s)	V_1 (m/s)	f_b	R_b (mm)	τ_b (N/m^2)	F	Re	Re^*
1	4	0.02	26	39.1	36.3	0.808	0.782	0.0764	31.8	6.22	1.35	91,191	507
2	4	0.02	27	39.4	36.6	0.803	0.795	0.0782	32.1	6.28	1.34	93,001	521
3	4	0.04	27	32.5	29.7	0.988	0.988	0.0866	26.9	10.53	1.83	99,023	675
4	4	0.04	27	32.5	29.7	0.988	0.995	0.0866	26.9	10.53	1.83	99,023	675
5	3	0.05	23.5	30.5	27.7	1.061	NA	0.0881	25.3	12.35	2.04	93,366	676
6	4	0.06	27	29.6	26.8	1.096	1.098	0.0969	24.7	14.49	2.14	101,832	791
7	4	0.06	27	29.6	26.8	1.096	1.103	0.0969	24.7	14.49	2.14	101,832	791
8	4	0.08	24	26.8	24.0	1.223	1.139	0.0933	22.2	17.40	2.52	97,912	811
9	2	0.082	28	26.9	24.1	1.220	1.180	0.0967	22.4	17.92	2.51	106,795	899
10	4	0.10	27	25.4	22.6	1.299	1.309	0.0982	21.1	20.64	2.76	106,151	945
11	4	0.10	27	25.4	22.6	1.299	1.304	0.0982	21.1	20.64	2.76	106,151	945

Note: A constant discharge of 4.5 L/s was used in all the tests.

greatly reduced the risk of damaging the sensitive CCD camera by the strong reflection at the free surface. The LED was operated in the PIV (double pulse) mode. The light exiting the LED was collimated into a light sheet using a cylindrical lens. The light sheet was directed downward through the free surface and aligned with the centerline of the flume. Unlike a laser light sheet, the LED light sheet was much thicker (≈10 mm). Hence, the measured velocities were spatially averaged in the transverse direction and could only be used to determine the mean velocities. Images of the illuminated "light sheet" were captured using a PowerView Plus 4 MP camera (2048 × 2048 pixels, 12-bit intensity dynamic range) equipped with a 105-mm/f2.8 Nikkor focal lens. The camera viewed the vertical light sheet through a sidewall of the flume. The firing of the LED and image capture was synchronized for frame straddling. The time interval between the straddled frames was 100μs and the repetition rate was 7.25 Hz. The measurement area was located at a channel distance of about 50 times the flow depth from the flume entrance where the boundary layer was fully developed. The maximum field of view (FOV) was 34 mm × 34 mm, and the spatial resolution was about 16μm/pixel. The camera's FOV was aligned parallel to the channel slope and extended from the bed to just below the free surface, except in Test 5, where the FOV covered a smaller portion of the water column.

A summary of the PIV measurements performed is presented in Table 2. A total of 11 tests were completed for six different flow conditions created by varying the channel slope from 2% to 10%. Five of the six flow conditions were repeated a second time (1 and 2, 3 and 4, 6 and 7, 8 and 9, and 10 and 11). Each test consisted of two or more successive runs separated by 1–2 min without stopping the flow. Most of the tests had 4 runs. A total of 200 velocity vector fields were captured in each run, except in Tests 5 and 9, in which 100 velocity fields were captured per run. PIV image processing was conducted using the *INSIGHT 4G* software by TSI. The dimensions of the interrogation regions were 64 pixels by 32 pixels with a 50% overlap. The spatial resolution was 0.53 mm in the streamwise direction and 0.27 mm in the "vertical" direction. Background image subtraction was used to increase the signal-to-noise ratio of the PIV images. In addition, ensemble correlation processing was employed to combine all the images in the same run to create a single vector field (INSIGHT 4G User's Guide 2011) representing the time-averaged or mean velocity field. A processing mask was used to exclude the region near the free surface and around the edges of the images. The percent of spurious vectors in the remaining area was less than 5%. A global range filter was used to remove spurious vectors, followed by vector validation using the local median. Missing vectors were replaced with neighborhood mean values, but no smoothing was applied. The validated velocity field contained between 44 and 56 vector columns in the streamwise direction. These were averaged together to produce a single column of vectors representing the space-averaged vertical velocity profile over the gravel bed. The velocity profiles from different runs in the same test were then averaged to produce an ensemble- and space-averaged velocity profile for finding the bed shear stress.

The uncertainty in the measured velocities can be estimated as $\delta x/\delta t$, where δx is the uncertainty in the water particle displacement and δt is the time interval between straddled frames. PIV correlation peak displacement may be assumed to be accurate to within 1/10th of a pixel (Kiger 2015). With the spatial resolution equal to 16μm/pixel and δt equal to 100 μs, the measured velocities were resolvable to 1.6 cm/s, which is well below the cross-sectional average velocities of around 1 m/s shown in Table 2. The measurement uncertainty could be reduced by increasing the value of δt used in PIV image capture, but at the expense of reducing the spatial resolution of the measured velocities in the streamwise direction, which would result in fewer vector columns for spatial averaging.

Procedure for Solitary Wave Experiment

The solitary wave experiment was carried out in the same tilting flume as that described in Ting (2006). The wave flume is 25-m long, 0.9-m wide, and 0.75-m deep. A solitary wave with a wave height of 0.17 m was generated in a constant depth of 0.4 m and then propagated immediately onto a 1 in 40 slope. PIV measurements were carried out, in which the measured wave height and still water depth were around 0.24 and 0.2 m, respectively, near the point of incipient wave breaking. A false bottom covered with a single layer of gravel was installed in the test section to create a rough bed 1.3-m long and 0.864-m wide. The same type of gravel as in the steady flow experiment was used in the solitary wave experiment, but the size distribution was reduced to particles passing the No. 4 sieve (4.75 mm) and retained on the No. 10 sieve (2.0 mm). The estimated d_{50} and d_{90} values were 3.95 and 4.6 mm, respectively, with 70% of the grains falling in the size range between 3.5 and 4.75 mm.

The same PIV system was used in the solitary wave experiment, but with a 200 mJ Dual Nd:YAG laser for illumination. Titanium dioxide (specific gravity 4.2, mean diameter 3.5 μm) was used as seeding particles. The laser was mounted underneath the flume. The light sheet passed through the Plexiglas bottom on the onshore side of the test section and was then redirected by a mirror mounted on the flume floor to illuminate the measurement area in front of the PIV camera. The arrangement was like that used in Ting and Beck (2019) for volumetric three-component velocimetry (V3V) measurements under breaking waves over a sediment-laden bed. The FOV of PIV measurements was 32 mm by 32 mm aligned parallel to the sloping bottom. A total of 20 runs were carried out under the same incident wave condition. In each run, 30 straddled frames were captured at a repetition rate of 7.25 Hz, corresponding to 4 s of image capture when the solitary wave was passing in front of the camera. Wave generation and image capture were triggered by a TTL signal generated by the data acquisition system. The timing of the trigger signal was determined by trial and error so that the peak velocity at the wave crest phase was captured in the sequence of PIV images. The time interval between straddled frames was 200μs. The dimensions of the interrogation regions for PIV image processing were 128 pixels by 32 pixels with a 50% overlap. The spatial resolution was 1 mm in the cross-shore direction and 0.25 mm in the "vertical" direction. As in the steady flow experiment, ensemble correlation processing was employed to combine all the PIV images at the same phase from different runs to produce an ensemble-averaged velocity field. Each velocity field contains 28 vector columns. These were averaged together to produce a single column of vectors. The resulting ensemble- and space-averaged (average) velocity profiles were used to determine the temporal variation of bed shear stress.

Results for Steady Flow Experiment

Fig. 2 shows a definition sketch of the y-coordinate system. The origin of the (x, y)-coordinates is located at the lower left-hand corner of the FOV of the PIV camera. The bottom of the FOV is at $y = 0$; the theoretical bottom of the gravel bed (from log-law fitting) at $y = y_0$, the top of the gravel bed (from PIV images) at $y = y_1$, and the approximate location of the free surface (from measured flow

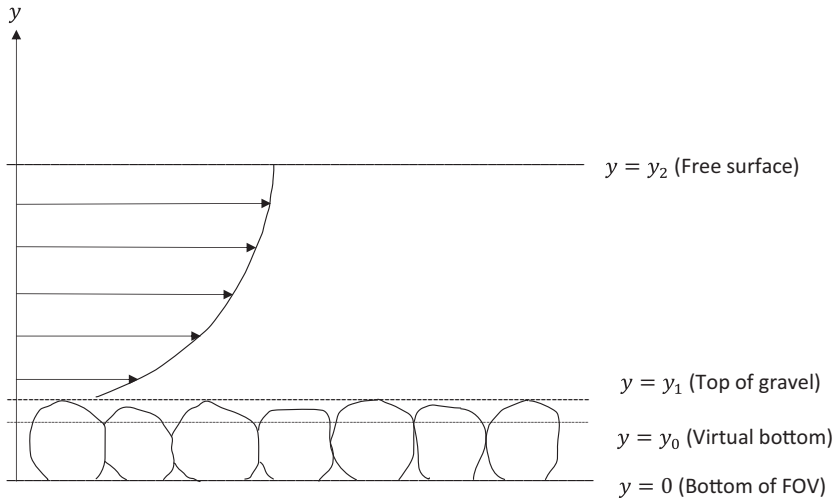

Fig. 2. Coordinate system for the gravel bed.

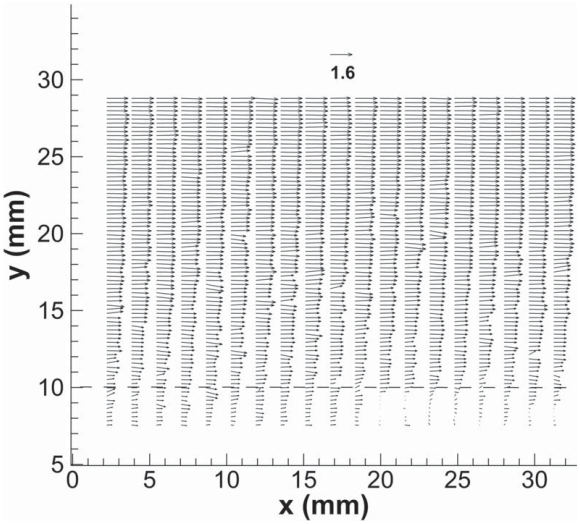

Fig. 3. Ensemble correlation velocity field (in m/s) from Test 8, Run 1. The top of gravel is indicated by the dashed line.

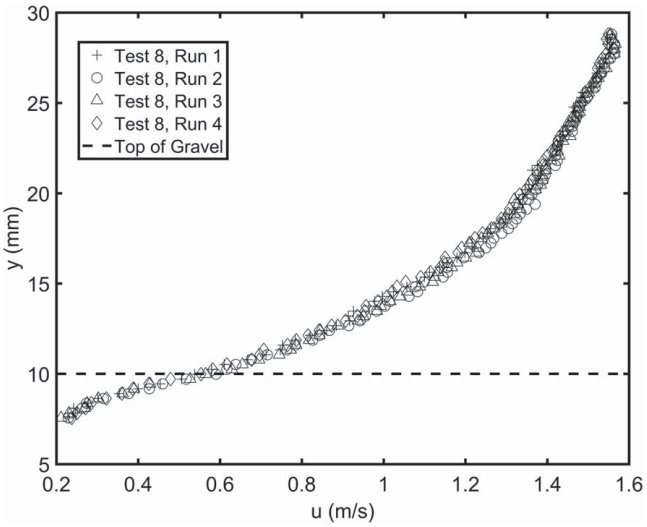

Fig. 4. Spatially averaged velocity profiles from Test 8, Runs 1–4.

depth) at $y = y_2$. Note that y_1 varied from test to test because the camera's FOV changed with the channel slope. Hence, the acrylic bed to which the gravel was adhered to could be inside the FOV (above $y = 0$). Fig. 3 shows the ensemble correlation velocity field from Test 8, Run 1. Only every three vector columns in the measured velocity field are shown to avoid cluttering. The dashed line marks the top of gravel. Below the dashed line, the flow was nestled among the particles. In the space occupied by the gravels, missing vectors were interpolated from neighborhood vectors. The free surface is located close to $y = 30$ mm. Fig. 4 shows the measured velocity profiles from four successive runs in Test 8. Each profile is the spatial average of 56 vector columns. The measured profiles show good repeatability and were averaged together to produce a single ensemble- and space-averaged (average) velocity profile for finding the bed shear stress.

Fig. 5 presents the average velocity profiles from Tests 2, 3, 5, 6, 8, and 11 as examples of the six different flow conditions investigated in this study. Except in Test 5, the velocity profiles were measured to within a few millimeters below the free surface, above which reflection from the LED light made accurate PIV measurements impossible. The measured velocity points in each profile were averaged to estimate the depth-averaged velocity. The results are given as V_1 in Table 2. The values are close to the cross-sectional average velocities denoted by V calculated from the measured discharge and flow depth. Also shown in each plot in Fig. 5 are the location of the theoretical bottom y_0, the top of the gravel bed y_1, and the approximate location of the free surface y_2. The theoretical bottom lies between 0.1 and $0.5d_{50}$ below the top of the gravel (Table 3), in general agreement with the value of 0.2–0.4 roughness diameter cited in the literature (Middleton and Southard 1984; Sumer and Fuhrman 2020).

The upper bound of the logarithmic profile is usually taken as no higher than 20%–30% of the flow depth above the bed, with the lower bound away from any direct influence of the roughness elements. Using Test 8 as an example, the top of the gravel is located approximately at $y = 10$ mm as indicated by the dashed line in Fig. 3. The log-law region is expected not to extend beyond around $y = 16$ mm. Nevertheless, one can fit Eq. (3) to more than one set of data points in this region. Fig. 6 presents plots of $y - y_0$ in the log

scale versus u with a best-fit line drawn to three different regions of the average velocity profile. The R^2 values of the best-fit lines are all greater than 0.995. The equivalent grain roughness is taken to be d_{65} (=6.1 mm), which yields a bed shear stress close to the value obtained from the measured flow depth and channel slope (Table 3). In Fig. 6(a), the best-ft line ($R^2 = 0.9985$) was obtained with 8 data points from $y - y_0 = 1.77$ to 3.65 mm ($y - y_1 = 0.52$ to 2.4 mm) and $y_0 = 8.75$ mm. The value of τ_b ($=\rho u^{*2}$) obtained from the slope of the best-fit line was 14.06 N/m^2. This result is dubious because the highest velocity point used for log-law fitting was only 2.4 mm ($<0.5d_{50}$) from the top of the gravel. The velocity profile this close to the bed would still be spatially disunified (Fig. 3). The bed shear stress obtained using the log law was about 19% lower than the value of 17.4 N/m^2 calculated from the measured flow depth and channel slope.

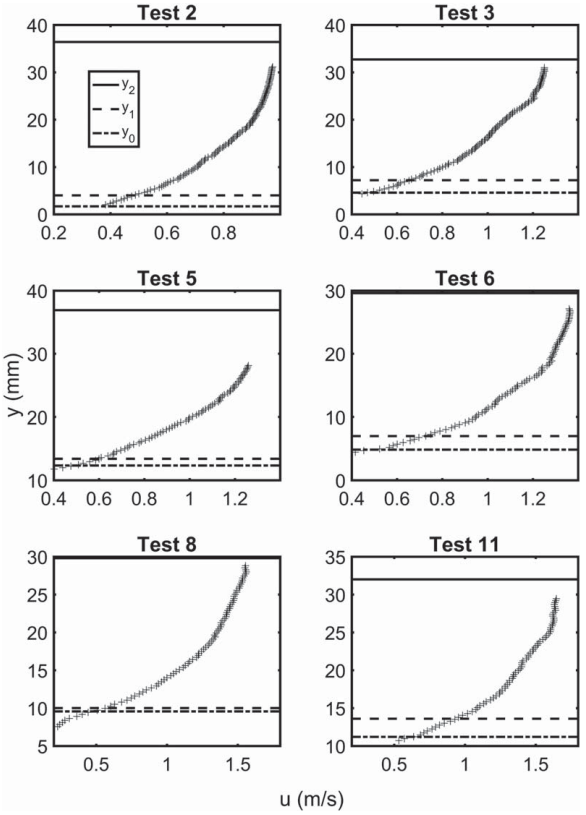

Fig. 5. Ensemble- and space-averaged (average) velocity profiles from Tests 2, 3, 5, 6, 8, and 11.

Away from the immediate vicinity of the bed, a best-fit line ($R^2 = 0.9954$) was obtained with 11 data points from $y - y_0 = 2.57$ to 5.25 mm ($y - y_1 = 2.14$ to 4.82 mm) and $y_0 = 9.57$ mm [Fig. 6(b)]. The value of τ_b obtained was 16.99 N/m^2, which was only 2.4% below the value calculated from the measured flow depth and channel slope.

Eq. (3) also fits the overlapping region between the inner and the outer layers well. Fig. 6(c) shows the best-fit line ($R^2 = 0.997$) obtained with 10 data points from $y - y_0 = 3.56$ to 5.98 mm ($y - y_1 = 4.01$ to 6.43 mm) and $y_0 = 10.45$ mm. The value of τ_b obtained is 19.49 N/m^2, which is 12% greater than the value calculated from the measured flow depth and channel slope.

Although the best-fit line shown in Fig. 6(c) is optimized for the inner layer, it also fits the velocity profile in the outer layer well. The h/d_{90} ratio in Test 8 was 3.6, so the gravel layer occupied a significant fraction of the flow depth. Middleton and Southard (1984) commented that at small values of the flow-depth-to-grain-size ratio, the distinction between the inner and the outer layers becomes blurred and the entire velocity profile would be affected by bottom roughness. The logarithmic profile would fit the velocity profile well through the entire flow depth provided that y_0 is adjusted appropriately. Note that y_0 is greater than y_1 when Eq. (3) is fitted to velocity points in the outer layer, which means that the theoretical bottom is above the top of the gravel.

Fig. 7 plots $y - y_0$ in the log scale versus u for the six tests shown in Fig. 5. The best-fit line in each plot was obtained by fitting Eq. (3) to the velocity points in the inner layer but away from the immediate vicinity of the bed. The number of data points used for log-law fitting was optimized to give an R^2 value equal to or greater than 0.995. The equivalent grain roughness was held constant at d_{84} in Tests 2, 3, and 5; d_{65} in Tests 6 and 8; and d_{50} in Test 11. The value of y_0 was varied until the von Kármán constant κ obtained from the y-intercept of the best-fit line was equal to 0.4. The resulting bed shear stress estimates were close to the values calculated from the measured flow depth and channel slope (Table 3). For Tests 10 and 11, which had the smallest measured h/d_{90} ratio (=3.4), the best-fit line in the inner layer also represented the velocity profile in the outer layer well. The bed shear stress value obtained by extending the best-fit line to the velocity points way out into the outer layer was only about 3% smaller than the value obtained from the inner layer. Table 3 summarizes the bed shear stress estimates obtained using the log law, τ_{b2}, with d_{50}, d_{65}, and d_{84} as the equivalent roughness height. The 95% confidence bounds are included in parenthesis for the d_r

Table 3. Bed shear stress obtained using the log law with different equivalent grain diameters

Test	Slope S	h/d_{90}	y_0, y_1, y_2 (mm)	$\tau_{b1} = \rho g R_b S$ (N/m^2)	τ_{b2}(log law) (N/m^2) d_{50}, d_{65}, d_{84} (95% CI)	$\frac{\tau_{b1} - \tau_{b2}}{\tau_{b1}} \times 100\%$ d_{50}, d_{65}, d_{84}
1	0.02	5.3	1.1, 4, 35.7	6.22	5.23, 5.41, 5.77 (5.64–5.89)	15.9, 13.0, **7.2**
2	0.02	5.3	1.7, 4, 36	6.28	5.62, 5.83, 6.21 (5.8–6.66)	10.5, 7.2, **1.1**
3	0.04	4.4	4.6, 7.2, 32.3	10.53	9.33, 9.73, 10.41 (9.7–11.21)	11.4, 7.6, **1.1**
4	0.04	4.4	4.8, 7.2, 32.3	10.53	9.55, 9.96, 10.66 (9.74–11.71)	9.3, 5.4, **−1.2**
5	0.05	4.1	12.3, 13.4, 36.5	12.35	11.4, 11.87, 12.7 (11.76–13.74)	7.7, 3.9, **−2.8**
6	0.06	4.0	4.9, 7, 29.2	14.49	13.4, 13.99 (12.84–15.33), 15.04	7.5, **3.5**, −3.8
7	0.06	4.0	4.9, 7, 29.2	14.49	13.64, 14.25 (12.21–16.88), 15.32	5.9, **1.7**, −5.7
8	0.08	3.6	9.6, 10, 29.4	17.40	16.28, 16.99 (15.37–18.88), 18.24	6.4, **2.4**, −4.8
9	0.08	3.6	5.3, 6, 25.5	17.92	15.21, 15.91, 17.1 (13.55–22.31)	15.1,11.2, **4.6**
10	0.10	3.4	11.1, 13.6, 31.6	20.64	21.19 (19.61–22.96), 22.1, 23.67	**−2.7**, −7.1, −14.6
11	0.10	3.4	11.2, 13.6, 31.6	20.64	20.87 (19.39–22.53), 21.75, 23.29	**−1.1**, −5.4, −12.8

Notes: y_0 = elevation of the theoretical bottom; y_1 = top of the gravel; and y_2 = approximate location of the water surface. The value of y_0 and the 95% confidence interval for τ_{b2} are given for the value of d_r that produces the smallest percent difference (in boldface) between τ_{b1} and τ_{b2}.

J. Waterway, Port, Coastal, Ocean Eng., 2022, 148(4): 04022008

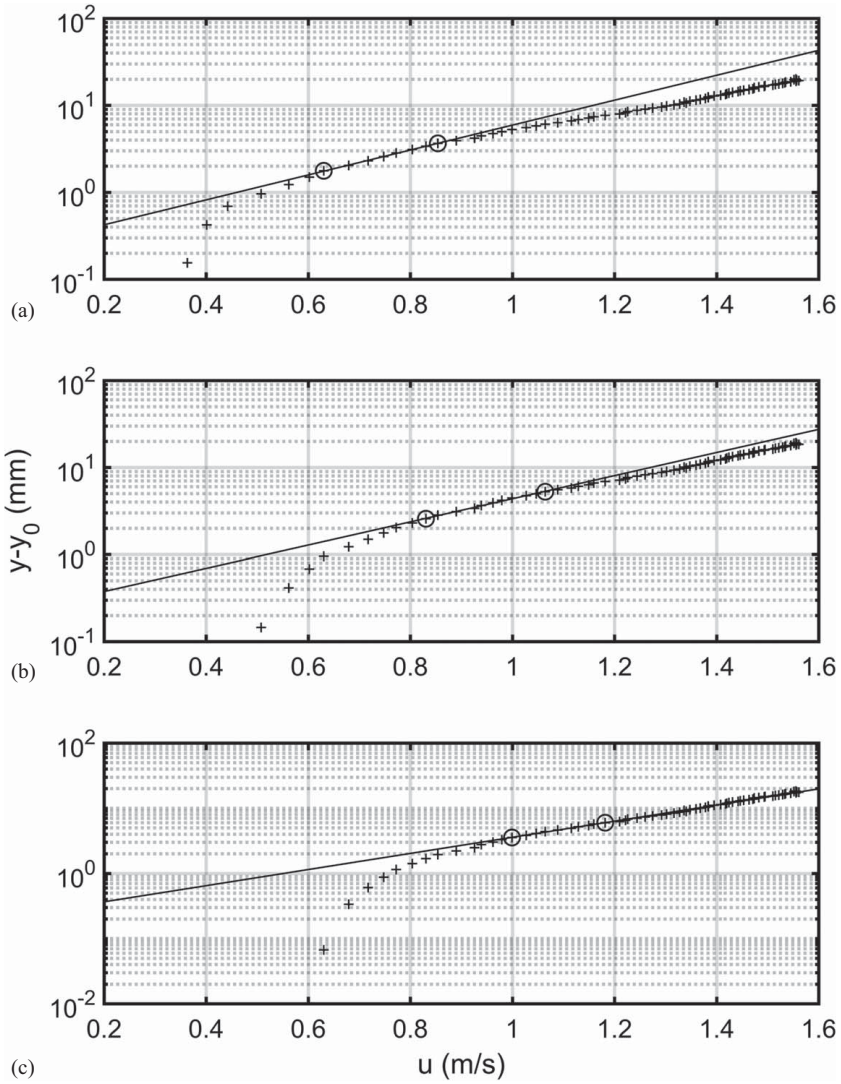

Fig. 6. Semilog plots of average velocity profile from Test 8 with the best-fit lines in different regions: (a) $y - y_1 = 0.52$–2.4 mm; (b) $y - y_1 = 2.14$–4.82 mm; and (c) $y - y_1 = 4.01$–6.43 mm. The end points of the log-law fitting are marked by circles. The value of k_s is 6.1 mm.

value that yields the best agreement between τ_{b1} and τ_{b2} in Table 3. Note that Test 9 had the highest measurement uncertainty for τ_{b2}. The velocity profile was computed from only two experiment runs, and, therefore, the data were noisier. Consequently, there were fewer accurately measured velocity points for log-law fitting.

The selection of the theoretical bottom y_0 affects the estimates for τ_b and k_s and is an important issue in finding the bed shear stress using the log law. The values of τ_{b2} given in Table 3 were obtained by holding k_s constant and varying y_0 systematically until the value of κ obtained from the y-intercept of the best-fit line was equal to 0.4. Using Test 8 as an example, we now show that this approach produces less variation in the values of u^* compared with the traditional method. Referring to Fig. 6(b), a value of 16.99 N/m^2 was obtained for τ_b from the slope of the best-fit line when $y_0 = 9.57$ mm. Based on the goodness of fit, there is no justification for selecting this y_0 value over other possible values. The R^2 values were all equal to or greater than 0.995 and the RMSD decreased monotonically with y_0 (Table 4). The correct value of τ_b cannot always be determined by comparing the R^2 and RMSD values at different y_0 values because these statistics are sensitive to uncertainty in the velocity measurements. Fig. 8 shows the variations of τ_b and k_s with y_0 obtained by fitting Eq. (3) to 11 data points from $y - y_0 = 2.57$ to 5.25 mm. This figure shows that as y_0 decreases, τ_b and k_s increase as we have discussed. The value of τ_b increases from 13.2 to 22.7 N/m^2 and the value of k_s from 3.6 to 10.4 mm (≈ 0.7–$2d_{50}$), when y_0 is decreased from 10 to 9 mm over a range of just 1 mm ($<0.2d_{50}$).

Instead of finding k_s with u^* when determining the value of y_0, k_s is held constant at d_{65} and only y_0 is varied. Fig. 9 shows the variations of κ and τ_b with y_0 obtained by fitting Eq. (3) to the same data points. The value of κ from the y-intercept of the best-fit line is equal to 0.4 when $y_0 = 9.57$ mm, and the corresponding value of τ_b obtained from the slope is 16.99 N/m^2. Values of κ between 0.35 and 0.43 are reported in the literature (e.g., Foken 2006). Fig. 9 shows that the variation of τ_b (from 16.3 to 17.3 N/m^2) with κ in this range is less than 5% of the expected value of τ_b. Comparing Fig. 9 with Fig. 8, it is found that the variation of τ_b with y_0 is much smaller by keeping the value of k_s constant.

The data plotted in Figs. 8 and 9 are tabulated in Table 4. This table illustrates how the friction velocity u^* is found. In the traditional method, the desired value of y_0 is found by maximizing the R^2 value and minimizing the RMSD of the best-fit line. The friction velocity u^* and equivalent roughness height k_s (Columns 4 and 6) are then found from the slope and y-intercept (Columns 2 and 3) of the best-fit line. This procedure is especially sensitive to uncertainty in the velocity measurements. In Test 8, all the R^2 values (Column 7) are around 0.995 and the RMSD (Column 8)

increases with y_0. Therefore, the correct value of y_0 cannot be determined by examining these statistics. There is a wide variation in the τ_b value (Column 5) with y_0. In the new method, k_s is held constant (Column 9) and y_0 is varied until the value of κ (Column 10) found from the y-intercept of the best-fit line is equal to 0.4. The bed shear stress τ_b (Column 12) obtained is much less sensitive to the value of y_0 selected. Both methods yield the same result for τ_b at $y_0 = 9.57$ mm. However, the new method provides a systematic way for finding u^* from the measured velocity profile, provided that the value of k_s is known or can be correctly estimated. The algorithm can be programmed easily for a given set of velocity points.

We carried out the aforementioned analysis using a range of d_r values as the equivalent roughness height. The results for d_{50}, d_{65}, and d_{84} are summarized in Table 3 and plotted in Fig. 10. There is a gradual shift to smaller values for k_s as the h/d_{90} ratio decreases and τ_b increases. In Tests 2–5, the best agreement between the bed shear stress estimates obtained from the measured flow depth and channel slope (τ_{b1}) and using the log law (τ_{b2}) is found when d_{84} is chosen as the equivalent roughness height, although the percent differences are still no more than 10% if d_{65} is used. In Tests 6–8, d_{65} provides a better choice for k_s. In Tests 10 and 11 ($h/d_{90} = 3.4$), the desired value of k_s is close to d_{50} (=5.6 mm), which yields $k_s/d_{90} = 0.76$. The latter is close to the value of 0.78 obtained at $h/d_{90} = 3.0$ by Kamphuis (1974). Both studies show that the value of k_s for $h/d_{90} < 10$ is significantly smaller than the value of $2.5d_{90}$ found in deeper channels. Therefore, the new method produces results consistent with published data.

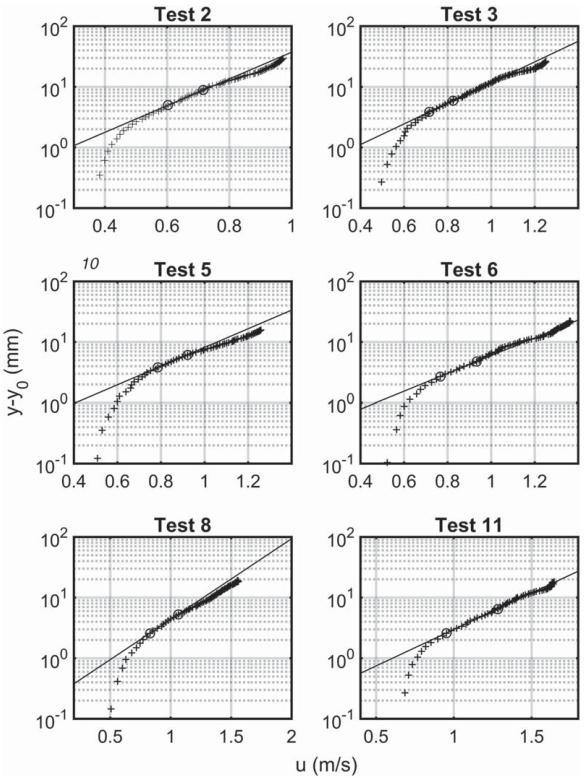

Fig. 7. Semilog plots of average velocity profiles from Tests 2, 3, 5, 6, 8, and 11 with the best-fit lines in the inner layer. The end points of the log-law fitting are marked by circles.

Results for Solitary Wave Experiment

The time series consists of 30 ensemble- and space-averaged velocity profiles (Frames 0–29) sampled at 7.25 Hz. Frame 0 is taken at $t = 0$ and Frame 29 at $t = 4$ s. Fig. 11 shows the average velocity profiles from Frames 10 to 21. The origin of the y-coordinate is taken at the bottom of FOV of the PIV images and the top of the gravel bed is located at approximately $y_1 = 5$mm. The maximum free-stream velocity is reached in Frame 14. After Frame 21, the fluid velocity adjacent to the bed reverses direction and moves in the opposite direction to the free-stream velocity (not shown). This phenomenon has been discussed in Liu et al. (2007). The effect of bottom friction on the velocity defect and growth of the boundary-layer thickness can be seen in the time evolution of the

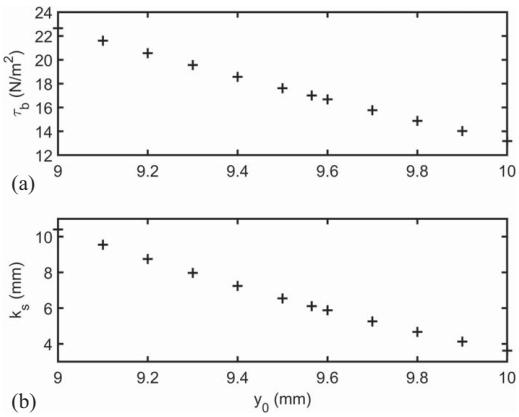

Fig. 8. Variations of (a) bed shear stress τ_b; and (b) equivalent roughness height k_s with displacement height y_0 in Test 8.

Table 4. Finding the friction velocity and bed shear stress in Test 8 of the steady flow experiment

y_0 (mm)	a (s/m)	b (m)	$u^* = \frac{\kappa}{a}$ (m/s)	$\tau_b = \rho u^{*2}$ (N/m^2)	$k_s = e^{(8.5\kappa+b)}$ (mm)	R^2	RMSD	k_s (mm)	$\kappa = \frac{(\ln k_s - b)}{8.5}$	$u^* = \frac{\kappa}{a}$ (m/s)	$\tau_b = \rho u^{*2}$ (N/m^2)
9	2.654	−7.966	0.1507	22.65	10.40	0.9957	0.01414	6.1	0.337	0.1271	16.10
9.1	2.718	−8.051	0.1472	21.60	9.55	0.9957	0.01453	6.1	0.347	0.1278	16.28
9.2	2.786	−8.139	0.1436	20.56	8.75	0.9956	0.01496	6.1	0.358	0.1284	16.43
9.3	2.856	−8.232	0.1401	19.56	7.97	0.9956	0.01543	6.1	0.369	0.1290	16.61
9.4	2.931	−8.328	0.1365	18.57	7.24	0.9955	0.01595	6.1	0.380	0.1296	16.75
9.5	3.01	−8.43	0.1329	17.61	6.54	0.9954	0.01652	6.1	0.392	0.1302	16.90
9.565	3.063	−8.498	0.1306	17.01	6.11	0.9954	0.01693	6.1	0.400	0.1305	16.99
9.6	3.093	−8.536	0.1293	16.68	5.88	0.9953	0.01717	6.1	0.404	0.1307	17.04
9.7	3.181	−8.648	0.1257	15.77	5.26	0.9952	0.01788	6.1	0.417	0.1312	17.18
9.8	3.275	−8.766	0.1221	14.88	4.67	0.9951	0.01869	6.1	0.431	0.1317	17.30
9.9	3.374	−8.89	0.1186	14.02	4.13	0.9949	0.01962	6.1	0.446	0.1322	17.42
10	3.48	−9.021	0.1149	13.18	3.62	0.9947	0.02062	6.1	0.461	0.1326	17.53

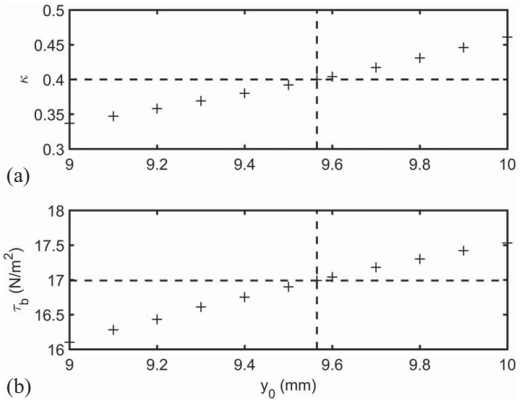

Fig. 9. Variations of (a) κ; and (b) τ_b with y_0 in Test 8 by holding k_s constant at the d_{65} value. The intersection of the horizontal and vertical dashed lines in (b) gives the values of τ_b and y_0 when $\kappa = 0.4$.

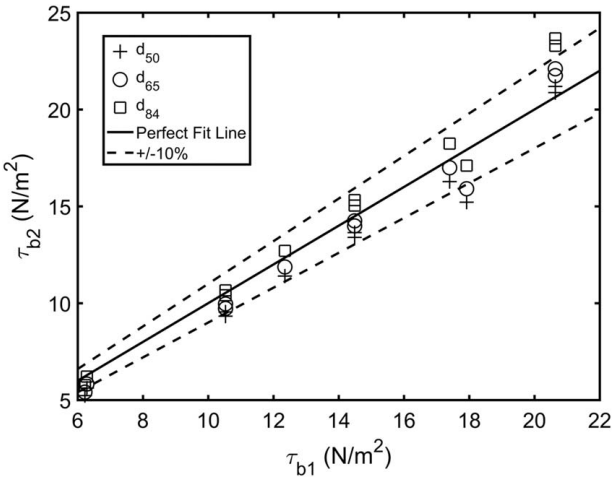

Fig. 10. Comparison of the bed shear stress values obtained using the log law τ_{b2} and from the measured flow depth and channel slope τ_{b1}.

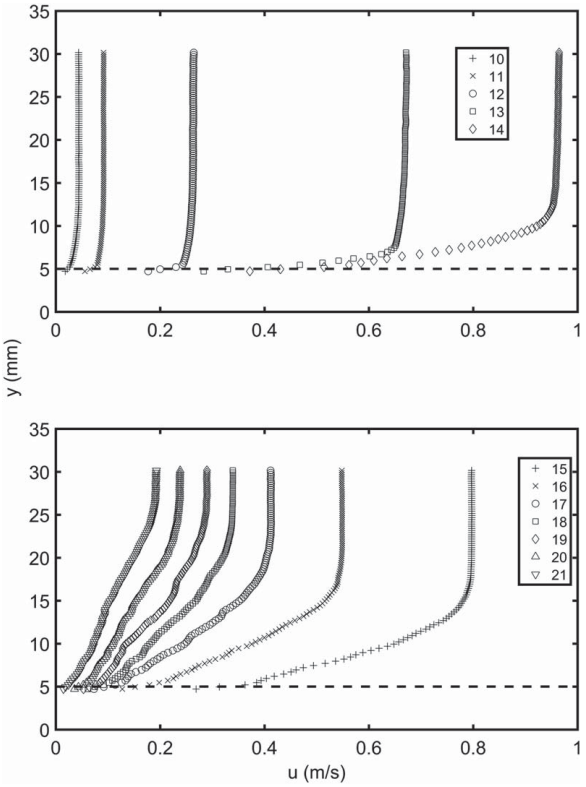

Fig. 11. Ensemble- and space-averaged velocity profiles under a solitary wave. The maximum free-stream velocity occurs in Frame 14. The top of the gravel is indicated by the dashed line.

velocity distribution. The measured velocity at the top of FOV is approaching the free-stream velocity and is taken to be the free-stream velocity u_0. A rough estimate of the thickness of the boundary layer δ in Frame 14 is around 10 mm.

To determine the value of k_s, Eq. (3) is fit to the average velocity profile in Frame 14 when the free-stream velocity is at the maximum. The largest straight-line portion of the velocity profile near the bed consists of eight data points between $y - y_1 = 1.2$ and 2.95 mm. The latter is within the limit of 0.3δ commonly taken to be the upper bound of the logarithmic layer. The displacement height y_0 is varied until R^2 and RMSD are close to their maximum and minimum values, respectively (Table 5). The values of y_0 and k_s obtained are 3.8 and 11.1 mm, which yield $k_s = 2.4d_{90}$ and $y_1 - y_0 = 0.26d_{90}$. The value of τ_b is 18.3 N/m^2, and the 95% confidence interval is between 17.1 and 19.7 N/m^2. The same value of k_s is applied to the instantaneous velocity profile from Frames 10 to 21, and y_0 is varied until the value of κ obtained from the y-intercept of the best-fit line is equal to 0.4. The friction velocity u^* is then found from the slope of the best-fit line. The results are summarized in Table 6. For Frame 14, the value of u^* obtained using the new method (Table 5, Column 11) is the same as that found using the traditional method (Table 5, Column 4) because the same velocity profile was used to determine the value of k_s.

When the new method was applied to a subset of velocity points used to find k_s, the values of y_0 and u^* obtained changed by only 1%–2%. This shows that the results from log-law fitting are not sensitive to the number of velocity points used if there are sufficient accurately measured points. In the new method, y_0 is treated as a fitting parameter. As discussed in Middleton and Southard (1984), the physical meaning of y_0 has never been clearly established. Although typical values may range from 0.2 to 0.4 roughness diameters below the top of the roughness elements, the actual value is very sensitive to uncertainty in the velocity measurements. The value of y_0 can vary from trial to trial on the same bed type. Therefore, the value obtained may be used only as a check. For example, a value of y_0 greater than y_1 (theoretical bed higher than the gravel bed) would mean that the log law has probably been fitted erroneously to velocity points above the inner layer.

The effect of varying y_0 on τ_b can be seen in Table 5. If the value of y_0 is taken to be 3.3 or 4.3 mm instead of 3.8 mm (Column 1), the value of τ_b will change from 18.3 to 18.6 and 18 N/m^2, respectively (Column 12). The changes in τ_b are insignificant, but they show that between y_0 and k_s, the latter is the important parameter that must be determined accurately to obtain the correct value of τ_b. The value of y_0 has little effect on τ_b and is best left as a fitting parameter to account for the uncertainties in the velocity measurements and the von Kármán constant.

If y_0 is held constant along with k_s, u^* will be the only parameter that can be adjusted in Eq. (3). For example, with $k_s = 11.1$ mm, $B = 8.5$, and $\kappa = 0.4$, solving Eq. (3) with the same set of velocity points in Frame 14 for κ/u^* by the method of least squares will yield $\tau_b = 16.1$, 18.3, and 21.5 N/m^2 for $y_0 =$ 3.3, 3.8, and 4.3 mm, respectively. Hence, a large difference in the value of τ_b may result if y_0 is determined from the velocity profile at one wave phase and then used with a different velocity profile to find the value of u^* at another wave phase. Therefore, y_0 may not be treated as a constant like k_s.

Table 5. Finding the friction velocity and bed shear stress at the wave crest phase (Frame 14) in the solitary wave experiment

y_0 (mm)	a (s/m)	b (m)	$u^* = \frac{\kappa}{a}$ (m/s)	$\tau_b = \rho u^{*2}$ (N/m^2)	$k_s = e^{(8.5\kappa+b)}$ (mm)	R^2	RMSD	k_s (mm)	$\kappa = \frac{(\ln k_s - b)}{8.5}$	$u^* = \frac{\kappa}{a}$ (m/s)	$\tau_b = \rho u^{*2}$ (N/m^2)
3.3	2.544	−7.456	0.1572	24.68	17.32	0.9983	0.007283	11.1	0.348	0.1367	18.64
3.4	2.616	−7.536	0.1529	23.34	15.99	0.9984	0.007269	11.1	0.357	0.1365	18.60
3.5	2.692	−7.62	0.1486	22.04	14.70	0.9985	0.007254	11.1	0.367	0.1363	18.55
3.6	2.772	−7.708	0.1443	20.78	13.46	0.9986	0.007240	11.1	0.377	0.1361	18.49
3.7	2.858	−7.801	0.1400	19.55	12.27	0.9987	0.007231	11.1	0.388	0.1358	18.42
3.8	2.949	−7.898	0.1356	18.36	11.13	0.9988	0.007233	11.1	0.400	0.1355	18.33
3.9	3.046	−8.002	0.1313	17.21	10.03	0.9988	0.007254	11.1	0.412	0.1352	18.25
4	3.15	−8.111	0.1270	16.10	9.00	0.9989	0.007305	11.1	0.425	0.1348	18.15
4.1	3.202	−8.187	0.1249	15.58	8.34	0.9986	0.007366	11.1	0.434	0.1354	18.31
4.2	3.329	−8.314	0.1202	14.41	7.34	0.9984	0.007966	11.1	0.449	0.1348	18.13
4.3	3.465	−8.451	0.1154	13.30	6.40	0.9983	0.008673	11.1	0.465	0.1341	17.96

Table 6. Summary of results in solitary wave

Frame	u_0 (m/s)	$y_1 - y_0$ (mm)	u^* (m/s)	τ_b (N/m^2)	R^2	RMSD	95% CI, τ_b (N/m^2)	k_s (mm)	Re^*
10	0.044	1.29	0.0074	0.054	0.9933	0.02430	0.035–0.096	11.1	81
11	0.092	1.37	0.0209	0.44	0.9971	0.01445	0.15–4.25	11.1	231
12	0.264	1.53	0.0585	3.42	0.9863	0.02932	1.85–8.29	11.1	648
13	0.672	1.35	0.1185	14.01	0.9988	0.00754	12.77–15.45	11.1	1,311
14	0.964	1.20	0.1355	18.33	0.9989	0.00650	17.12–19.70	11.1	1,502
15	0.797	1.92	0.0788	6.20	0.9971	0.00818	5.36–7.25	11.1	871
16	0.548	1.45	0.0467	2.18	0.9960	0.01017	1.84–2.62	11.1	516
17	0.412	0.65	0.0333	1.11	0.9941	0.01973	0.98–1.26	11.1	369
18	0.339	1.65	0.0233	0.54	0.9973	0.01095	0.48–0.62	11.1	258
19	0.290	1.87	0.0180	0.32	0.9996	0.00287	0.30–0.35	11.1	200
20	0.238	1.55	0.0139	0.19	0.9906	0.02675	0.16–0.23	11.1	154
21	0.192	0.99	0.0081	0.07	0.9967	0.01889	0.05–0.08	11.1	90

Note: Water density and kinematic viscosity are computed at a water temperature of 20°C.

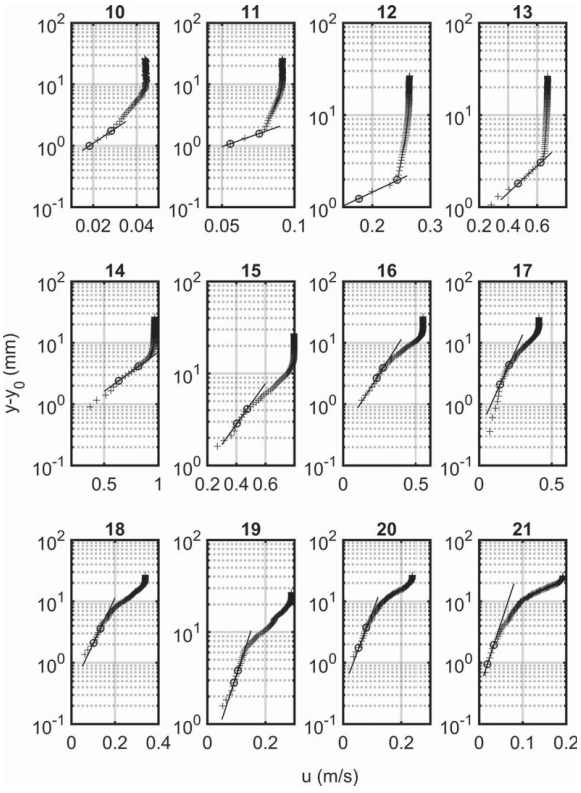

Fig. 12. Semilog plots of average velocity profiles under the solitary wave with the best-fit line in the inner layer. The end points of the log-law fitting are marked by circles.

Table 6 summarizes the results from Frames 10 to 21 when a logarithmic region can be found. The values of $y_1 - y_0$ range from 0.65 to 1.92 mm, or between 0.14 and 0.42 d_{90} below the top of the gravel. The values of Re^* are all greater than 60, and, therefore, the wave-induced flow over the gravel bed was hydraulically rough. Fig. 12 plots $y - y_0$ in the log scale versus u for the velocity profiles shown in Fig. 11. The best-fit line in each plot was obtained by fitting Eq. (3) to the largest straight-line region that could be found in the inner layer. The logarithmic region is very thin before Frame 13, and, therefore, the 95% confidence bounds are large. Fig. 13 shows the variations of the wave elevation η, free-stream velocity u_0, longitudinal pressure gradient dp/dx, and bed shear stress τ_b with time. The wave profile shown is the average of five successive runs, and the sampling interval is 12 ms. The measured wave height and still water depth are 0.237 and 0.198 m, respectively. Wave breaking occurred just shoreward of the test section where the measured breaker height index was close to 1.2.

Due to the low sampling rate of the PIV measurements, the fluid velocity and bed shear stress values between the measured points in Fig. 13 were interpolated by spline fitting. The results show that the maximum bed shear stress occurs 0.04 s ahead of the maximum velocity. The method employed by van der A et al. (2011) in acceleration-skewed flow was used to estimate the wave friction factor. The effective wave orbital amplitude in the free stream is calculated as $a = 2S(T_1/T_2)$, where $S = 0.6$ m is the stroke of the wavemaker and $T_1/T_2 \approx 0.25$ is the ratio of the duration of the positive flow acceleration to the duration of positive flow velocity measured using two cutoff points shown in the velocity profile for u_0 in Fig. 13. The relative roughness a/k_s is about 30, which yields a value of 0.04 for the wave friction factor f_w (see Fig. 21 in van der A et al. 2011). The predicted bed shear stress $\tau_b (= 1/2\rho f_w u_0^2)$

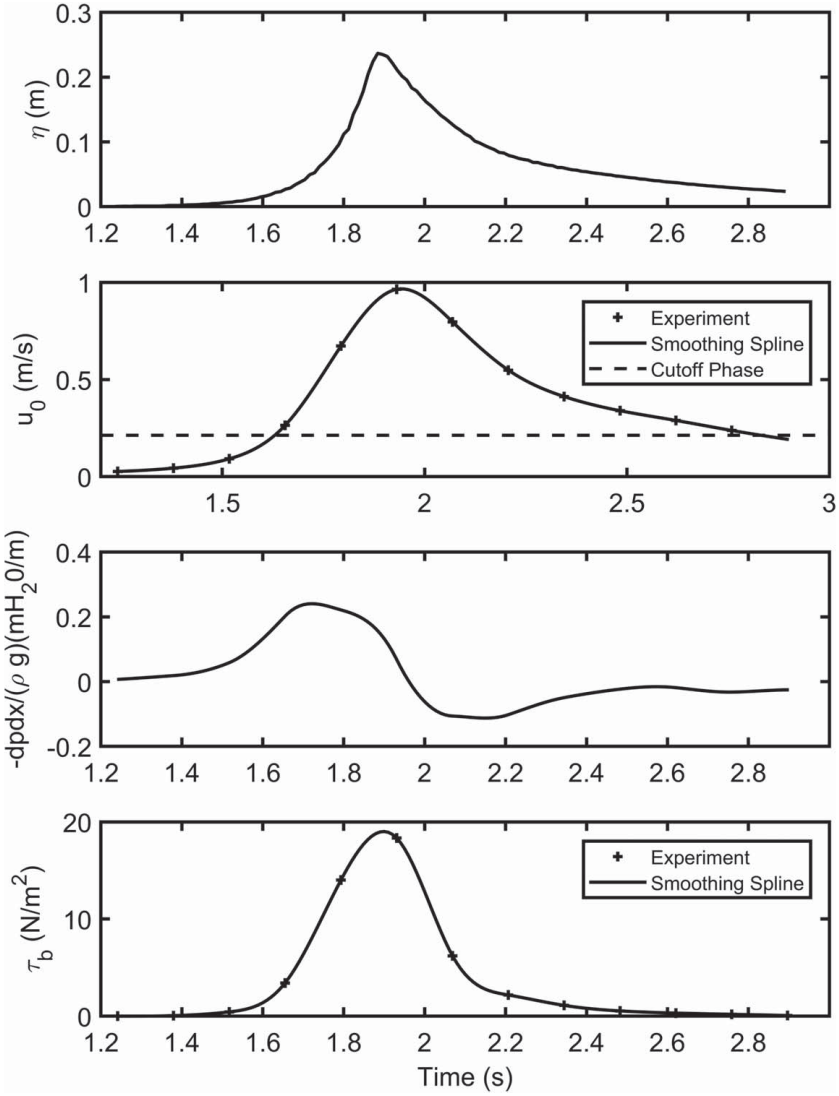

Fig. 13. Variations of water surface profile, free-stream velocity, longitudinal pressure gradient, and bed shear stress with time for the solitary wave.

is equal to 18.6 N/m^2, which is close to the value obtained using the log law.

Also plotted in Fig. 13 is the temporal variation in the longitudinal pressure gradient dp/dx ($=-\rho Du/Dt$) in the free stream. The local acceleration term $\partial u/\partial t$ was computed as the first derivative of the spline curve for u_0. The maximum wave-induced longitudinal pressure gradient occurs under the wave front and is around 0.2 mH$_2$O/m. This result is consistent with published data (Baldock 2012).

Conclusions

An alternative method for finding the bed shear stress from a measured velocity profile on a hydraulically rough bed is presented. The method assumes that the von Kármán constant is a universal constant, and the equivalent roughness height is known. The measured velocity profile is graphed on a plot of $\ln(y-y_0)$ versus u and the displacement height y_0 is varied until the value of κ obtained from the y-intercept of the best-ft line is equal to 0.4. The friction velocity u^* is then found from the slope of the best-fit line. This method avoids finding u^* by varying both y_0 and k_s simultaneously. The traditional method of optimizing the logarithmic fit by trial and error is cumbersome, and the results are very sensitive to the value of y_0 selected. The new method converges rapidly, and the value of u^* obtained is relatively insensitive to the known variation in the κ value. The method was applied to a steady uniform flow over a fixed layer of fine gravel at small values of the h/d_{90} ratio. By matching the values of τ_b obtained using this method with those computed from the measured flow depth and channel slope, it was found that the values of the k_s/d_{90} ratio agreed well with the experimental data by Kamphuis (1974), thus verifying that the results produced by the method were correct. The new method was then applied to the measured velocity profiles under a solitary wave to obtain the temporal variation of bed shear stress near the point of incipient breaking. The maximum bed shear stress obtained was in good agreement with the value computed using the wave friction factor for acceleration-skewed oscillatory flow.

The method described in this paper is most useful in an unsteady flow in which the bed shear stress varies with time and in a steady, nonuniform flow in which it may be difficult to determine the energy slope. In oscillatory flows and surface waves, the traditional method of varying y_0, u^*, and k_s simultaneously to optimize the logarithmic fit would lead to temporal variations in the equivalent bed roughness, which is unrealistic if the boundary layer is fully turbulent, and the bed is hydraulically rough. In addition, the results are very sensitive to the value of y_0 selected. Hence, it would be difficult

to distinguish between the temporal variation in u^* from the uncertainty associated with selecting the y_0 value. The traditional method works well when there are many accurately measured velocity points, but it can produce high uncertainty in the results when the logarithmic region is thin, as is during rapid flow acceleration. A better approach is to obtain a good estimate of k_s by applying the traditional method at the wave crest or wave trough phase when the flow is quasi-steady and the logarithmic region is relatively thick (van der A et al. 2011; O'Donoghue et al. 2021). The method described in this paper can then be used to determine the intrawave friction velocity with greater efficiency and consistency.

Appendix. Side Wall Correction of Bed Shear Stress

The bed shear stress in a steady flow is computed using the procedure described in Vanoni and Brooks (1975) and improved by Cheng (2011). For a uniform flow in a rectangular channel with smooth side walls, the bed shear stress τ_b can be computed using the following equations:

$$\tau_b = \rho g R_b S \tag{5}$$

$$R_b = \frac{f_b}{f} R \tag{6}$$

$$f_b = f + 2\frac{h_e}{b}(f - f_w) \tag{7}$$

$$f = \frac{8gRS}{V^2} \tag{8}$$

$$f_w = 31\left[\ln\left(1.3\frac{Re}{f}\right)\right]^{-2.7} \tag{9}$$

where ρ = fluid density; g = acceleration of gravity; R_b = bed-related hydraulic radius; S = channel slope; f = bulk friction factor; f_b = bed friction factor; f_w = wall friction factor; h_e = effective flow depth; b = channel width; $R(=bh_e/(b+2h_e))$ = hydraulic radius; $V(=Q/(bh_e)$ = cross-sectional average velocity; $Re(=V(4R)/\nu)$ = Reynolds number; and ν = kinematic viscosity. The effective flow depth h_e is computed as follows (Ferreira et al. 2012):

$$h_e = h - (1 - n)D \tag{10}$$

where h = flow depth measured from the acrylic sheet to which the gravel was adhered; n = porosity of the gravel; and D = thickness of the gravel layer. Values of $n = 0.5$ and $D = d_{50}$ are assumed in this study.

Data Availability Statement

All data presented in this paper are available from the corresponding author upon reasonable request.

Acknowledgments

Funding for this study was provided by the United States Department of Transportation (USDOT) to the Mountain-Plains Consortium (MPC). Additional funding was provided by the National Science Foundation (NSF) through Grant No. OCE-2049293. The support of the MPC and the NSF is gratefully acknowledged.

Notation

The following symbols are used in this paper:

A, B = integration constants in the log law;
a, b = slope and y-intercept of the best-fit line;
b = channel width [Eq. (7)];
D = representative grain size or diameter of uniform grains;
d_r = grain diameter with r% of finer particles;
F = Froude number;
f = bulk friction factor;
f_b = bed-related friction factor;
f_w = wall friction factor;
g = acceleration of gravity;
h = flow depth;
h_e = effective flow depth;
k_s = equivalent grain roughness;
n = porosity;
p = pressure;
R = hydraulic radius;
R_b = bed-related hydraulic radius;
Re = Reynolds number;
Re^* = boundary Reynolds number;
S = channel slope;
t = time;
u = mean velocity;
u_0 = free-stream velocity;
u^* = friction velocity;
V = cross-sectional average velocity;
V_1 = depth-averaged velocity;
y = vertical coordinate;
y_0 = elevation of the theoretical bottom;
y_1 = top of the gravel bed;
y_2 = water surface elevation;
α = the multiplying factor;
δ = boundary-layer thickness;
η = wave elevation;
κ = von Kármán constant;
ν = kinematic viscosity;
ρ = fluid density; and
τ_b = bed shear stress.

References

Baldock, T. E. 2012. "Discussion of 'laboratory investigation of pressure gradients induced by plunging breakers', by Pedrozo-Acuña et al." *Coast. Eng.* 66: 1–2. https://doi.org/10.1016/j.coastaleng.2012.03.008.

Cheng, N.-S. 2011. "Revisited Vanoni–Brooks sidewall correction." *Int. J. Sediment Res.* 26 (4): 524–528. https://doi.org/10.1016/S1001-6279(12)60010-9.

Cox, D. T., N. Kobayashi, and A. Okayasu. 1996. "Bottom shear stress in the surf zone." *J. Geophys. Res.* 101 (C6): 14337–14348. https://doi.org/10.1029/96JC00942.

Dixen, M., F. Hatipoglu, B. M. Sumer, and J. Fredsøe. 2008. "Wave boundary layer over a stone-covered bed." *Coast. Eng.* 55 (1): 1–20. https://doi.org/10.1016/j.coastaleng.2007.06.005.

Ferreira, R. M. L., M. J. Franca, J. G. A. B. Leal, and A. H. Cardoso. 2012. "Flow over rough mobile beds: Friction factor and vertical distribution of the longitudinal mean velocity." *Water Resour. Res.* 48 (5): W05529. https://doi.org/10.1029/2011WR011126.

Frings, R. M., H. Schüttrumpf, and S. Vollmer. 2011. "Verification of porosity predictors for fluvial sand–gravel deposits." *Water Resour. Res.* 47 (7): W07527. https://doi.org/10.1029/2010WR009690.

Foken, T. 2006. "50 years of the Monin–Obukhov similarity theory." *Boundary Layer Meteorol.* 119: 431–447. https://doi.org/10.1007/s10546-006-9048-6.

INSIGHT 4G User's Guide. 2011. *Insight 4G global imaging, acquisition, analysis and display software*. Shoreview, MN: TSI.
Jensen, B. L., B. M. Sumer, and J. Fredsøe. 1989. "Turbulent oscillatory boundary layers at high Reynolds numbers." *J. Fluid Mech.* 206: 265–297. https://doi.org/10.1017/S0022112089002302.
Kamphuis, J. W. 1974. "Determination of sand roughness for fixed beds." *J. Hydraul. Res.* 12 (2): 193–203. https://doi.org/10.1080/00221687409499737.
Kiger, K. 2015. "PIV basics: Correlation." In *SEDITRANS summer school on measurement techniques for turbulent open-channel flows*. http://www.civil.ist.utl.pt/~ruif/SUMMER_SCHOOL/presentations/PIV_basics_correlation_final.pdf.
Liu, P. L.-F., Y. S. Park, and E. A. Cowen. 2007. "Boundary layer flow and bed shear stress under a solitary wave." *J. Fluid Mech.* 574: 449–463. https://doi.org/10.1017/S0022112006004253.
López, R., and J. Barragán. 2008. "Equivalent roughness of gravel-bed rivers." *J. Hydraul. Eng.* 134 (6): 847–851. https://doi.org/10.1061/(ASCE)0733-9429(2008)134:6(847).
Middleton, G. V., and J. B. Southard. 1984. *Mechanics of sediment movement*. 2nd ed. SEPM Society for Sedimentary Geology. Short Course Number 3. Tulsa, OK: Society of Economic Paleontologists and Mineralogists.
Nikuradse, J. 1933. "Strömungsgesetze in Rauhen Rohren." *VDI-Forschungsheft* 361. [In English.] *NACA Tech. Mem*. 1292.
O'Donoghue, T., A. G. Davies, M. Bhawanin, and D. A. van der A. 2021. "Measurement and prediction of bottom boundary layer hydrodynamics under modulated oscillatory flows." *Coast. Eng.* 169: 103954. https://doi.org/10.1016/j.coastaleng.2021.103954.
Sleath, J. F. A. 1987. "Turbulent oscillatory flow over rough beds." *J. Fluid Mech.* 182: 369–409. https://doi.org/10.1017/S0022112087002374.
Sumer, B. M., and D. R. Fuhrman. 2020. *Turbulence in coastal and civil engineering*, 731. Singapore: World Scientific.
Ting, F. C. K. 2006. "Large-scale turbulence under a solitary wave." *Coast. Eng.* 53: 441–462. https://doi.org/10.1016/j.coastaleng.2005.11.004.
Ting, F. C. K., and D. A. Beck. 2019. "Observation of sediment suspension by breaking-wave-generated vortices using volumetric three-component velocimetry." *Coast. Eng.* 151: 97–120. https://doi.org/10.1016/j.coastaleng.2019.03.009.
van der A, D. A., T. O'Donoghue, A. G. Davies, and J. S. Ribberink. 2011. "Experimental study of the turbulent boundary layer in acceleration-skewed oscillatory flow." *J. Fluid Mech.* 684: 251–283. https://doi.org/10.1017/jfm.2011.300.
Vanoni, V. A., and N. H. Brooks. 1957. *Laboratory studies of the roughness and suspended load of alluvial streams*. Pasadena, CA: Sedimentation Laboratory, California Institute of Technology.
Xie, M., C. Zhang, J. Li, S. Li, Z. Yang, and H. Zhang. 2021. "Flow structure and bottom friction of the nonlinear turbulent boundary layer under stormy waves." *Coast. Eng.* 164: 103811. https://doi.org/10.1016/j.coastaleng.2020.103811.
Yuan, J., and O. S. Madsen. 2014. "Experimental study of turbulent oscillatory boundary layers in an oscillating water tunnel." *Coast. Eng.* 89: 63–84. https://doi.org/10.1016/j.coastaleng.2014.03.007.
Zarrati, A. R., and Y. C. Jin. 2004. "Discussion of 'Response of velocity and turbulence to sudden change of Bed roughness in open-channel flow' by Xingwei Chen and Yee-Meng Chiew" *J. Hydraul. Eng.* 130 (6): 586–587. https://doi.org/10.1061/(ASCE)0733-9429(2004)130:6(586).